RSC Advances

ROYAL SOCIETY OF CHEMISTRY

www.rsc.org/advances

Preparation, characterization and gas separation properties of nanocomposite materials based on novel silane functionalizing polyimide bearing pendent naphthyl units and ZnO nanoparticles

Mohammad Dinari * and Hashem Ahmadizadegan

Organic Polymer Chemistry Research Laboratory, Department of Chemistry, Isfahan University of Technology, Isfahan, 84156-83111, I. R. Iran.

Abstract

* Corresponding author. Tel.; +98-31-3391-3270; FAX: +98-31-3391-2350.

E-mail address: dinari@cc.iut.ac.ir, mdinary@gmail.com (M. Dinari).

The novel diamine with naphthyl pendent group was prepared by the nucleophilic substitution reaction of 5-methylnaphthalen-1-amine and 4-fluoronitrobenzene followed by the reduction with hydrazine monohydrate and a Pd/C. An aromatic polyimide (PI) with silane end group was synthesized and the hybrid nanocomposite films of the PI with silane end groups and different amounts of zinc oxide were successfully fabricated and characterized by different techniques. Thermogravimetry analysis indicated that the hybrid films had high thermal stability. Transmission electron microscopy of nanohybrid films show that the ZnO phase is well dispersed in the polymer matrix. Mechanical properties of PI/ZnO nanocomposite films increased with increased ZnO content. The gas separation properties of the hybrid membranes were study and the results show that the permeation of N_2, O_2, CH_4 and CO_2 has been increased in comparison with pristine PI membrane.

Keywords: Polymer-matrix composites; Nano-structures; Mechanical properties; Thermal analysis; Gas separation

1. Introduction

A varied range of polymer and inorganic have been combined to form nanocomposite (NC) materials with unique properties such as mechanical, electrical, magnetic and adhesive.[1-4] The top candidate to be hosting matrices for composite materials is polymeric materials due to their ability to yield a variety of properties. Furthermore, organic polymers usually have long-term stability and good flexibility.[5] However, polymers have some disadvantages such as poor thermal and electrical properties and have lower modulus and strength in comparison with metals and ceramics.[6,7] Different methods, such as synthesis of homopolymers, copolymers, and modified

polymers were performed but they were not sufficient to compensate various properties, which were required.[8-10] On the other hand, inorganic nanoparticles possess excellent optical, catalytic, electronic, and magnetic properties.[11-14] By combining these two components, NCs derived from organic polymers and inorganic nanoparticles are expected to increase properties.[15,16] In general, these resulting organic polymer-based inorganic nanoparticle composites have been used in several fields such as electronics, coatings, and catalysis.[17-21] In the choice of polymeric matrix, several properties such as chemical stability and chemical functionalities should be examined. Polyimides (PI)s as a high performance polymers, are good candidates for these purposes because of their significant properties such as high temperature stability, good chemical resistance, excellent mechanical properties and hydrogen bonding interaction.[22-26] One of the problems with high-performance PIs is their poor solubility or processability, and they do not react below their decomposition temperature; this restricts their applications as engineering materials.[27,28] To overcome these limitations, synthetic suggests have been centered on increasing their solubility in organic solvents without sacrificing the above mentioned outstanding properties. New synthetic techniques have been focused on improving processability and solubility through the synthesis of new diamine or dianhydride monomers. Attempts in this field include introduction of bulky substituents, flexible linkage, and structurally unsymmetrical segments into the polymer backbone.[29-32]

Among different inorganic nanoparticles, ZnO is one of the most potential materials in research and application fields because of its versatile functions. Due to the expected properties of ZnO, considerable attention has been devoted to the manufacture of well-dispersed ZnO in polymer matrix used as interference filter, antireflective coating, and optical waveguides.[33-36] ZnO with hexagonal wurtzite structure is one of the multifunctional inorganic semiconductors

that have drawn increasing attention in recent years due to its many significant potential application in solar cells, gas sensors, varistors, piezoelectric devices, electro-acoustic, and transducers, chemical absorbent, UV light emitting devices, sun-screens, UV absorbers, and electrostatic dissipative coating. Furthermore, ZnO is an environmentally friendly material and has little toxicity.[37-39]

In the present investigation, novel PI/ZnO hybrid thin films were prepared from ZnO nanoparticles and PI-bearing Si-OH end groups. The Si-OH end groups could condense with ZnO nanoparticles and provide organic–inorganic hybrids. Thus, no additional coupling agents would have to be used in the preparation of the hybrid materials. The physical, thermal, and gas separation properties of these novel mixed matrix membranes were studied and we expect that these novel hybrid materials could be equipped with good gas separation properties, solubility and thermal stability.

2. Experimental

2.1. Materials

All chemicals were purchased from Fluka Chemical Co. (Buchs, Switzerland), Aldrich Chemical Co. (Milwaukee, WI), and Merck Chemical Co. Pyromelliticdianhydride (PMDA) was recrystallized from acetic anhydride and then dried in a vacuum oven at 120 °C overnight. Dimethyl sulfoxide (DMSO), *N,N′*-dimethylacetamide (DMAc) and *N*-methyl-2-pyrrolidone (NMP) were dried over barium oxide. ZnO nanoparticle with an average particle size of about 25–30 nm was purchased from Neutrino Co (Tehran, Iran).

2.2. Equipments

Proton and carbon nuclear magnetic resonance (^{1}H-NMR, 500 MHz and ^{13}C-NMR, 125 MHz) spectra were recorded in DMSO-d_6 solution using a Bruker (Germany) Avance 500 instrument. Proton resonances are designated as singlet (s), doublet (d), and multiplet (m). The chemical composition of the intermediates and obtained particles was studied by FT-IR spectroscopy using a Jasco-680 FT-IR spectrophotometer (Japan) in the spectral range between 4,000 and 400 cm^{-1} with KBr pellet. Vibration bands were reported as wavenumber (cm^{-1}). The band intensities are assigned as weak (w), medium (m), shoulder (sh), strong (s), and broad (br). The XRD patterns were recorded by using a Philips Xpert MPD diffractometer equipped with a Cu Kaanode (k = 0.154056 nm at 40 kV and 30 mA) in 2θ range of 10°–80° at the speed of 0.05° min^{-1}. A UV/vis spectrum was measured on UV/Vis/NIR spectrophotometer, JASCO, V-570 with solid pellets of the samples in the spectral range between 200 and 800 nm. Thermal properties of the polymer and the NCs were studied on STA503 TA instrument in nitrogen atmosphere at a heating rate of 10 °C min^{-1}. Differential scanning calorimetry (DSC) was taken by Perkin-Elmer DSC-7 in nitrogen atmosphere at a heating rate of10 °C min^{-1}. FE-SEM micrographs of samples were taken on a Hitachi (S-4160). The morphology and dispersity analysis was performed on TEM analyzer on Philips CM 120 operating at 100 kV. The NC films were first microtomed into 60 nm ultra thin sections with a diamond knife using Leica Ultracut UCT ultramicrotome. The mechanical properties were measured on a Testometric Universal Testing Machine M 350/500 (UK), consistent by means of ASTM D 882 (standards). Tests were carried out through a cross-head speed of 12.5 mm/min until/to a deformation of 20% and then at a speed of 50 mm/min at break. The gas permeability of the polymer membranes with thickness around 30 μm was measured with a automated Diffusion Permeameter (DP-100-A) manufactured by Porous Materials Inc., USA, which consists of upstream and downstream parts separated by a

membrane. The reproducibility of the measurements was checked from three independent measurements using the same membrane and it was better than ±5% for CO_2 and O_2 permeability measurement but the reproducibility was in the range of ±10% for CH_4 and N_2 permeability measurements.

2.3. Synthesis of diamine monomer

In a 50 mL three-neckround-bottom flask was placed, 1.0 g (6.29 mmol) of 5-methylnaphthalen-1-amine (1), 1.76 g (12.60 mmol) of 4-fluoronitrobenzene, 2.56 g (19 mmol), of cesium fluoride and 15 mL of DMSO. The mixture was heated with stirring at 110 °C for 8 h under nitrogen atmosphere. The reaction mixture was cooled and then poured into 250 mL of ethanol. The creamy precipitate was collected by filtration and dried under vacuum. The product was purified by recrystallization from glacial acetic acid to afford 5-methyl-*N,N*-bis(4-nitrophenyl)naphthalen-1-amine (3) in 90% yield; mp 208-2210 °C. Hydrazine monohydrate (3 mL) was added dropwise to a mixture of compound 4 (1.0 g, 2.5 mmol), ethanol (40 mL), and a catalytic amount of 10% palladium on activated carbon (Pd/C, 0.03 g) at the boiling temperature. The mixture became homogeneous after 1 h, and the reaction was refluxed for 28h. The mixture was then filtered to remove Pd/C. After cooling, the precipitated blue crystals were isolated by the recrystallization from ethanol and the yield was 78%; mp 175- 177 °C.

FTIR (KBr, cm^{-1}): 3455 (s), 3388 (s), 3117 (w), 3090 (w), 2920 (w), 1576 (m), 1555 (m) 1449 (w), 1366 (w), 1169 (w), 833 (m), 765 (w).

^{1}H-NMR (500 MHz, DMSO-d_6, ppm): 3.03 (s, 3H, CH), 4.64 (s, 4H, NH), 6.67 (d, 8H, Ar-H, *J*= 4.5 Hz), 6.96 (d, 1H, Ar-H), 7.37 (d, 1H, Ar-H),7.69 (dd, 2H, Ar-H, *J*= 4 Hz), 7.77 (d, 1H, Ar-H, *J*= 4 Hz), 7.88 (d, 1H, Ar-H, *J*= 4 Hz).

^{13}C-NMR (125 MHz, DMSO-d_6), δ (ppm): 28.58 (CH_3), 107.15 (Ar), 109.29 (Ar), 111.62 (Ar), 114.69 (Ar), 125.50 (Ar), 126.00 (Ar), 128.47 (Ar), 129.75 (Ar), 131.25 (Ar), 134.85 (Ar), 138.33 (Ar), 143.65 (Ar), 147.47 (Ar).

Elemental analysis calculated for $C_{23}H_{21}N_3$ (339.17g mol^{-1}): Calcd: (%) C, 81.38%; H, 6.24 %; N, 12.38%. Found: C, 81.46%; H, 6.29 %; N, 12.19%.

2.4. Synthesis of PI with Si-OH end groups

Firstly, 2.037 g (0.006mol) of diamine monomer 4 was added into a 100ml three-necked round bottom flask and 38 ml of DMF was used to dissolve the reactants. 2.617 g (0.012mol) of PMDA was then slowly added into the above solution with vigorous stirring under nitrogen purging. The mixture was allowed to react for 10 h at room temperature to formed poly(amic acid) with anhydride end group. Secondly, 2.054 g (0.012mol) of *p*-aminophenyltrimethoxysilane (APhTMOS) and 9.6 ml of 1,3-dichlorobenzene were added to the above solution. The PAA solution with silane end group was thus formed after constantly stirring the reactants for 14 h at room temperature. The PAA solution was then thermally imidized in 180 ^{o}C silicon oil bath for another 18 h and cooled to room temperature. The homogeneous PI–SiOH solution was precipitated with 50 ml of methanol and re-dissolved in 40 ml of THF twice. A white-gray precipitate was recovered and dried in a vacuum oven at 150°C for 24 h to obtain 2.73 g of PI-SiOH. The inherent viscosity of the PAA at concentration of 0.5 g/dL at 30 ^{o}C in DMF was 1.12 dL/g.

2.5. Synthesis of PI/ZnO hybrid thin films

0.1 g of PI–SiOH was dissolved in 3ml of DMAc and different amounts of ZnO nanoparticles were added to the solution with a syringe. The mixture was then stirred at room temperature for

30min to obtain the precursor solution of PI/ZnO (5, 10, and 15%). Thin films of PI with different percentages of ZnO precursor were fabricated by casting onto dust-free glass plates. Resulted thin films were annealed using an electric air-circulating oven at 60, 120, 170, 220, and 270°C for 1 h each and 300°C for 12 h and then were cooled and removed from glass surface using a sharp edge blade. The prepared PI/ZnO hybrid thin films were examined using different techniques.

3. Results and discussion

3.1. Synthesis and characterizations of diamine monomer

A diamine monomer containing naphthyl pendent groups was synthesized according to the synthesis pathway which was shown in Scheme 1. In the first step, aromatic nucleophilic substitution reactions of 5-methylnaphthalen-1-amine with 4-fluoronitrobenzene in the presence of CsF in DMSO resulted in intermediate dinitro compound 3. In the second step, the dinitro compound was reduced to the corresponding diamine 4 in the presence of Pd/C and hydrazine. The chemical structure and purity of the diamine was confirmed by elemental analyses, FT-IR, ^{1}H NMR and ^{13}C NMR spectroscopy techniques and the results are reported in the experimental section. In the FT–IR spectrum of diamine, characteristic bonds of amino groups at 3447–3383 cm^{-1} (N–H stretching vibrations) and 785 cm^{-1} (N–H out of plane bending) appeared after reduction and the characteristic absorptions of dinitro at 1370 and 1525 cm^{-1}, were disappeared.

Scheme 1

The ^{1}H-NMR spectrums confirm the proposed structure for diamine 4. As shown in Fig. 1, the methyl group on the naphthyl ring is presented at 3.00 ppm, the amino groups are appears at around 4.61-4.63 ppm and the aromatic protons are presented in the range of 6.67-7.85 ppm. Fig. 2 shows the ^{13}C

NMR spectrum of the diamine 4. The aliphatic carbons are presented at 28.58 ppm and the aromatic carbons are presented in the range of 107.10–147.50 ppm.

Fig. 1

Fig. 2

3.2. Synthesis of PI/ZnO hybrid films

Aromatic PI with silane end group was synthesized from the condensation of aromatic diamine with naphthyl pendent group as well as APhTMOS and aromatic dianhydride by two-step condensation polymerization method, that is, the formation of PAA followed by a thermal imidization of this compound in the presence of different amount of ZnO nanoparticles to give PI/ZnO hybrid films according to Scheme 2.

Scheme 2

3.3. Characterization of the hybrid films

3.3.1. FTIR study

The formation of PI and PI/ZnO hybrid materials was confirmed by FT-IR analysis (Fig. 3). For PAA, the characteristic broad absorption at 3440-3290 cm^{-1} due to the amino (N H) and hydroxyl (OH) groups, and amic carbonyl absorption at 1678 cm^{-1} was observed (Fig. 3e). The PAA film was heated to convert it to PI. The thermal imidization of amic-acid to imide ring was confirmed by the disappearance of 1675 cm^{-1} (amic acid C=O) and a new characteristic absorption of the imide group at 1766 cm^{-1} (C=O asym., str.), 1717 cm^{-1} (C=O sym., str.), and 1355 cm^{-1} (C–N str.) in the spectrum (Fig. 3d). The mentioned peaks were characteristic of absorption of the imide group and have been shown in the spectra of the PI film and PI/ZnO hybrid films. It is also found that the infrared spectrum of the coupling agent (APhTMOS)

treated ZnO nanoparticles exhibits absorptions at 3422 cm^{-1} (–OH), 2973 cm^{-1} (Si–OH), 940 cm^{-1}, (Zn–O–Si), and 850 cm^{-1} (Si–O–Si). The introduction of inorganic components can be observed in the strong, broad absorption bands in the range of 400–700 cm^{-1} corresponding to Zn–O–Zn network (Figs. 3a-3c).

Fig. 3

3.3. X-ray diffraction

Fig. 4 displays the XRD patterns of the PI and PI/ZnO hybrid films with different amount of ZnO nanoparticles. According to the Fig. 4, PI was totally amorphous in nature, which did not show any sharp diffraction peaks. The XRD pattern of NCs shows characteristic peaks of ZnO indicating that the crystallinity of ZnO nanoparticles was not changed during the preparation process and the intensity of diffraction peaks increases with increasing ZnO content. The average particle size of nanoparticles was estimated based on Scherrer correlation of particle diameter (D) $D=K\lambda/\beta\cos\theta$, where K is the Scherrer constant, λ the X-ray wavelength, β the peak width at half-maximum, and θ is the Bragg's diffraction angle. The average crystallite size of the ZnO calculated from the width of the diffraction peak according to the Scherrer equation is approximately less 48 nm. This is in agreement with the size of used ZnO nanoparticles.

Fig. 4

3.4. Morphology image studies (FE-SEM and TEM)

The morphology of the PI/ZnO NCs was investigated using both TEM photographs and FE-SEM techniques. According to the FE-SEM photographs, PI/ZnO NC5% and PI/ZnO NC15% reveal that the ZnO nanoparticles were homogeneously dispersed in the polymer matrix and the average particle size of the nanoparticles was in the range of 35–45 nm (Fig. 5a-5d). TEM has confirmed to be a powerful tool for studying the dispersion of nanofillers embedded within a

polymer matrix. The TEM micrograph of the PI/ZnO NC5% and PI/ZnO NC15% shows that nanoparticles were homogeneously dispersed in polymer matrix and no aggregation was observed in the TEM images of the NC films (Fig. 6a-6d). The nanoparticles might be dispersed absolutely and will combine with PI via the covalent bonding of OH nanoparticles with Si-OH end groups in PI. In addition, OH groups on the surface of ZnO nanoparticle can bond to the amide group (C=O) of PI through interchange hydrogen bonding. The obtained results indicate that Si-OH end groups in PI play an important role in the dispersion of nanoparticles into the polymer matrix.

Fig. 5

Fig. 6

3.5. TGA and DSC study

The thermal stability of the PI and NC with various ZnO nanoparticle contents was evaluated by TGA at 10 °C/min in nitrogen atmosphere. The TGA curves are shown in Fig. 7, and the thermal stability data determined from the original TGA curves are listed in Table 1. No weight loss was detected until the temperature was scanned up to 418 °C. The onset of decomposition temperature (temperature at 10% weight loss; T_d) was found to increase for all the resulting NCs. The T_d for PI/ZnO NC5% , PI/ZnO NC10% and PI/ZnO NC15% is around 448, 496 and 532 ^oC, respectively while for pure PI, it is 416 ^oC. The onset of decomposition temperature is higher by 32 ^oC than that of virgin PI (Fig. 7). In addition, it is also evidently to see that the more ZnO nanoparticles percentages have led to the more char yields at 800 °C in the resulting hybrid films. The char yield of the pure PI is 67 %, although that the PI/ZnO NCs with 5, 10 and 15 wt.% of ZnO nanoparticles were 74, 77 and 81 %, respectively (Table 1). Overall, the resulting NCs have better thermal stability than that of PI. The stronger bonding between the ZnO

nanoparticles and the PI with Si-OH network could be the direct reason for the difference of the films. Also, increasing in the thermal stability in NCs is attributed to the high heat resistance exerted by the ZnO, because the ZnO nanoparticles have high thermal stability so coupling of ZnO nanoparticles can improve the thermal stability of the NCs. The experimental results indicated that the NC films possessed great thermal stability to withstand the harsh environments of many high-tech applications such as microelectronic manufacturing and packaging industry.

Fig. 7

Table 1

The glass transition temperatures (T_g) values of NCs were determined using DSC analysis which showed the rising trend with the increasing of ZnO percentage as summarized in Table 1. The restriction of segmental movement due to the quite strong interaction between PI matrix and ZnO nanoparticles may well be the main reason for the increase in T_g values.

3.6. Mechanical properties

It is well known that the mechanical behavior of multiphase materials, such as filled and reinforced polymers, is closely related to the degree of interfacial adhesion between their components.[40,41] So, the effect of adding ZnO nanoparticles on PI matrix is related with the interactions of molecules in the hybrid films. Tensile properties of the PI/ZnO hybrids films were studied by typical stress strain curves. Specific values of the ultimate properties and the modulus of these samples are shown in Fig. 8 and the results are listed in Table 2. In comparison with the pure PI, NC with different amount of ZnO nanoparticles has higher ultimate strength; higher initial Young's modulus, but lower ultimate elongation. Filler consisting entirely of ZnO generally increases the ultimate strength, but decreases the maximum extensibility. Ultimate

strength and initial modulus were increased with ZnO contents, but ultimate elongation decreased sharply with the increase of ZnO contents, especially at lower ZnO content. The strength should be reduced if there are no bonding sites between the organic polymer phase and the inorganic ZnO phase. This is presumably due to the inert nature of the PIs and the weak interactions between these polymers and the ZnO. In this case, the ZnO acts as nonreactive, non-reinforcing filler. The ultimate properties of the NCs are dependent on different parameter such as: the extent of bonding between the polymer matrix as continuous phase and filler as discontinuous phase, the surface area of the ZnO, and the arrangements between the ZnO particles. The above results showed that the interactions between the PI matrix and the ZnO nanoparticles are very important in the preparation of the hybrid materials.

Fig. 8

Table 2

3.7. Gas separation performance test

The permeability of oxygen, nitrogen, methane and carbon dioxide was determined using constant pressure/variable volume method at 4, 8 and 12 bar pressures and at 25 ^{o}C.[42] The gas permeability of membranes was determined using the following equation (1):

$$P = \frac{ql}{A(p_1 - p_2)} \qquad (1)$$

where P is permeability expressed in Barrer (1 Barrer = 10^{-10} cm^3 (STP) cm/cm^2 s cmHg), q is flow rate of the permeate gas passing through the membrane (cm^3/s), l is membrane thickness (cm), p_1 and p_2 are the absolute pressures of feed side and permeate side, respectively (cmHg) and A is the effective membrane area (cm^2).

The ideal selectivity, $\alpha_{A/B}$ (the ratio of pair gas permeabilities) of membranes was calculated from pure gas permeation experiments according to the following equation (2):

$$\alpha = \frac{P_A}{P_B} \quad (2)$$

Permeation of N_2, O_2, CH_4 and CO_2 gases through PI and PI–ZnO hybrid membranes was inspected at room temperature and under the pressures of 4, 8 and 12 bar. The permeability results are shown in Figs. 9-12 and the results are also summarized in Table 3. As can be seen in Table 3, the permeability of gases in pure PI varies in the following order: CO_2> O_2> CH_4> N_2, while the order of gas permeability in hybrid membranes changed to CO_2> CH_4> O_2> N_2. Based on the well-known solution-diffusion mechanism, the permeability of gases through nonporous polymer membranes is defined as a combination of diffusion and solution processes. The differences in the gas permeabilities measured for pure PI is due to molecular size variations of the gases except for CH_4 and N_2. Generally speaking, the smaller size molecules can diffuse faster and as a result, have higher permeabilities; however, in the case of CH_4 and N_2 in spite of the smaller size of the nitrogen molecules, methane, thanks to its superior condensability, exhibits a higher amount of permeability. On the other hand, in this case the solubility mechanism can be regarded as the dominated mechanism in permeation of gases through PI polymer membranes. As could be inferred from Figs. 9-12, incorporation of ZnO nanoparticles results in a further increase in the permeability of methane to the amounts even higher than the oxygen. This is due to the fact that ZnO nanoparticles are able to increase the permeation of gases through the membrane by emphasizing the solubility domination in the permeation mechanism. As can be seen in Figs. 9-12, the permeability of all gases for the hybrid membranes has been increased in comparison with PI membrane. The reason for the increase in the gas

permeabilities of the prepared hybrid membranes is twofold: The first one is increasing the gas diffusivity in the membranes. The increase in the permeability of condensable CH_4 and CO_2 gases for hybrid membranes is considerably higher than that of noncondensable O_2 and N_2 gases. As discussed, by incorporation of ZnO particles in hybrid membranes domination of solubility mechanism in membranes increased and more condensable gases permeate faster due to their higher solubility ability in polymer. The comparison between CO_2 and CH_4 permeabilities reveals that the permeation of carbon dioxide is more enhanced by incorporation of the ZnO particles in the membranes. This can be attributed to an increased solubility of CO_2 in the hybrid membranes. The extensive affinity of the residual OH groups on the ZnO to the polar CO_2 molecules makes a major contribution to an increased interaction between carbon dioxide molecules and the membrane matrix leading to an enhanced solubility and accordingly an improved permeability of CO_2 in comparison with methane.

Permeability results obtained at different pressures indicate that for pure PI and hybrid PI/ZnO membranes, the permeability of N_2 and O_2 remains almost constant upon increasing the upstream pressure or the pressure difference. Nevertheless, permeability of CH_4 increases slightly and that of CO_2 significantly, by increasing the upstream pressure from 4 to 12 bars. The main reason for such a behavior can most likely be the increased solubility of condensable CO_2 and CH_4 molecules at higher pressures. Table 4 summarizes the ideal selectivity of various gases. The reported results represent an increase in the selectivity of CO_2/N_2 and CO_2/CH_4 upon increasing the pressure in PI and PI/ZnO hybrid membranes. This can be attributed to the enhanced solubility and plasticizing effect of CO_2 molecules in membranes at higher feed pressures. Also as could be inferred from Table 4, CO_2/N_2 and CO_2/CH_4 selectivities show an increase over 60 and 48%, respectively, with increasing ZnO content under all experimented

pressures whereas the O_2/N_2 selectivity does not follow a regular trend of increase or decrease with the ZnO content. This is most likely due to the solubility selectivity. As mentioned earlier, by increasing the ZnO content in hybrid membranes, the available sorption sites and pathways at the interfaces and in the ZnO domains for the polar gases increase. As a result, α CO_2/N_2 and α CO_2/CH_4 considerably increases with increasing ZnO content, resulting mainly from the superior solubility selectivity of polar CO_2 gas, while α O_2/N_2 does not change significantly because the solubility of O_2/N_2 remains nearly constant. Based on the condensability difference of CH_4 and N_2, the increase observed in the selectivity of CO_2/N_2 is considerably higher than that of CO_2/CH_4. As the content of ZnO in hybrid membranes is increased, the solubility of condensable CH_4 gas is also raised, whereas the solubility of noncondensable N_2 gas does not change significantly.

Permeability coefficient (P) of the neat PI and NC with different amount of ZnO nanoparticles were compared with the Matrimid[43] and the results are summarized in Table 4. According to this Table, for Matrimid the value of the P_{CO2} is 8.70 Barrers, but for PI with 0, 5, 10 and 15 wt% of ZnO nanoparticles, the permeability is 19.80, 24.99, 29.02 and 34.22 Barrers, respectively. Also for Matrimid, P_{CH4} is 0.24 and in the NC membrane it was increased from 5.03 to 6.91 Barreres. Another data are collected in Table 4.

Table 3

Table 4

Figs. 9-12

4. Conclusions

The synthesis and full characterization of a new diamine monomer containing aromatic rings are presented. PI/ZnO hybrid thin films were successfully prepared using a PI with Si-OH end

groups and ZnO nanoparticles. FT-IR and XRD results confirm the formation of ZnO particles in the PI matrix. According to UV-vis spectra, neat PI film and NCs with different ZnO nanoparticles showed good optical transparency with light transmittance at 500 nm of as high as 80% and cutoff wavelength of as low as 400 nm. The thermal analysis depicts the percentage of the inorganic material in an organic matrix. The thermal stability of the PI/ZnO NCs has increased compared to that of pure PI. TEM images confirmed nanoscale and homogeneous dispersion of nanoparticles in the polymer matrix. The mechanical properties of the PI and related NCs were investigated and the results show that the ultimate strength and initial modulus were increased with ZnO contents, but ultimate elongation decreased sharply with the increase of ZnO contents, especially at lower ZnO content. The gas separation properties of PI membrane with three ZnO concentrations (5, 10 and 15 wt%) are tested for gas permeation. Permeation of N_2, O_2, CH_4 and CO_2 gases through PI–ZnO hybrid membranes was increased in comparison with PI membrane and the order of gas permeability in hybrid membranes is CO_2> CH_4> O_2> N_2. Also CO_2/N_2 and CO_2/CH_4 selectivities show an increase over 60 and 48%, respectively, with increasing ZnO content under all experimented pressures, whereas, the O_2/N_2 selectivity does not follow a regular trend of increase or decrease with the ZnO content.

Acknowledgements

We wish to express our gratitude to the Research Affairs Division Isfahan University of Technology (IUT), Isfahan, for partial financial support. Further financial support from National Elite Foundation (NEF) and Iran Nanotechnology Initiative Council (INIC) is gratefully acknowledged.

References

1 G. Kickelbick, *Prog. Polym. Sci*., 2003, **2**, 83-114.

2 K. Rajeswar, N.R. Tacconi, C.R. Chenthamarakshan, *Chem. Mater*., 2001, **13**, 2765-2770.

3 X. Hu, H. Cong, Y. Shen, M. Radosz, *Ind. Eng. Chem. Res*., 2007, **46**, 1547-1551.

4 S. Mallakpou, M. Dinari, M. Hatami, *RSC Adv*., 2014, **4**, 42114-42121.

5 M. Bruma, F. Mercer, B. Schulz, R. Dietel, J. Fitch, P. Cassidy, *High Perform. Polym*., 1994, **6**, 183-191.

6 M.K. Ghosh, K.L. Mittal, *Polyimides: fundamentals and applications*. New York: Marcel Dekker, 1996.

7 M.J. Abadie, B. Sillion, *Polyimides and other high-temperature polymers*. Amsterdam: Elsevier, 1991.

8 B. Lin, X. Xu, *Polym. Bull*., 2007, **59**, 243-250.

9 L.S. Nair, C.T. Laurencin, *Prog. Polym. Sci*., 2007, **32**, 762-798.

10 S. Mallakpour, M. Khani, Polym Bull 2007, **59**, 587-596.

11 S.P. Sun, K.Y. Wang, N. Peng, T.A. Hatton, T.S. Chung, *J. Membr. Sci*., 2010, **363**, 232-242.

12 H. Althues, J. Henle, S. Kaskel, *Chem. Soc. Rev*., 2007, **36**, 1454-1465.

13 K. Ding, Z. Miao, Z. Liu, Z. Zhang, B. Han, G. An, S. Miao, Y. Xie. *J. Am. Chem. Soc*., 2007, **129**, 6362-6363.

14 S.C. Liufu, H.N. Xiao, Y.P. Li, *Polym. Degrad. Stab*., 2005, **87**, 103-110.

15 D. Pradhan, M. Kumar, Y. Ando, K.T. Leung, *J. Phys. Chem. C*., 2008, **112**, 7093-7096.

16 M. Dinari, H. Ahmadizadegan, Polymer, 2014, **55**, 6252-6260.

17 I. Gill, *Chem. Mater*., 2001, **13**, 3404-3421.

18 R. Murugan, S. Ramakrishna, *Biomaterials*, 2004, **25**, 3829-3835.

19 Y. Zhao, F. Wang, Q. Fu, W. Shi, *Polymer*, 2007, **48**, 2853-2859.

20 A. Hilonga, J.K. Kim, P.B. Sarawade, H.T. Kim, *Powder Technol*., 2010, **199**, 284-288.

21 H. Wu, W. Hou, J. Wang, L. Xiao, Z. Jiang, *J. Power Sources*, 2010, **195**, 4104-4113.

22 K. Chen, X.C. Kazuaki, Y.N. Endo, M. Higa, K. Okamoto, *Polymer,* 2009, 50, 510-518.

23 H. Wang, W. Zhong, P. Xu, Q. Du, *Composites Part A*., 2005, **36**, 909-914.

24 E. Marand, Q. Hu, *Polymer*, 1999, **40**, 4833-4843.

25 V.E. Yudin, J.U. Otaigbe, S. Gladchenko, B.G. Olson, S. Nazarenko, E.N. Korytkova, V.V. Gusarov, *Polymer*, 2007, **48**, 1306-1315.

26 Y. Xiong, X. Lu, *J. Polym. Res*., 2010, **17**, 273-277.

27 J. de Abajo, J.G. de la Campa, In; *Processable aromatic polyimides*; Kricheldorf HR, Ed. Springer: Berlin, 1999; pp 23-61.

28 S. Mallakpour, M. Dinari, *Iran. Polym. J*., 2011, **20**, 259-279.

29 T.M. Long, T.M. Swager, *J. Am. Chem. Soc*., 2003, **125**, 14113-14119.

30 M. Adnan Saeed, Z. Akhter, M. Saifullah Khan, N. Iqbal, M. Saeed Butt, *Polym. Degrad. Stab.*, 2008, **93**, 1762-1769.

31 M. Ghaemy, R. Alizadeh, H. Behmadi, *Eur. Polym. J*., 2009, **45**, 3108-3115.

32 D.Y. Zhu, L.X. Gao, M.X. Ding, Z.H. Yang, *Polymer*, 2012, **53**, 5706-5716.

33 Q. Wu, X. Chen, P. Zhang, Y. Han, X. Chen, Y. Yan, S. Li, *Cryst. Growth Des*., 2008, **8**, 3010-3018.

34 R. Rhodes, M. Horie, H. Chen, Z. Wang, M.L. Turner, B.R. Saunders, *J. Colloid Interface Sci*., 2010, **344**, 261-271.

35 S.K. Gupta, A. Joshi, M. Kaur, *J. Chem. Sci*., 2010, **122**, 57-62.

36 C.D. Corso, A. Dickherber, W.D. Hunt, *Biosens. Bioelectron*., 2008, **24**, 805-811.

37 Z.L. Wang, *Appl. Phys. A*., 2007, **88**, 7-15.

38 Y.Q. Li, S.Y. Fu, Y.W. Mai, *Polymer*, 2006, **47**, 2127-2132.

39 A. Becheri, M. Durr, P.L. Nostro, P.J. Baglioni, *J. Nanopart. Res*., 2008, **10**, 679-689.

40 Z. Ahmad, F. Al Sagheer, A. Al Arbash, A.A.M. Ali, *J. Non-Cryst. Solids*, 2009, **355**,507-517.

41 J. Lin, Y. Liu, W. Yang, Z. Xie, P. Zhang, X. Li, H. Lin, G. Chen, Q. Lei, *J. Polym. Res*., 2014, **21**, 531-538.

42 M.A. Semsarzadeh, M. Sadeghi, M. Barikani, H. Moaddel, *Iran. Polym. J*., 2007, **16**, 819-827.

43 M.D. Guiver, G.P. Robertson, Y. Dai, F. Bilodeau, Y.S. Kang, K.J. Lee, J.Y. Jho, J. Won, *J. Polym. Sci. Part A: Polym. Chem*., 2002, **40**, 4193-4204

Legends for Schemes

Scheme 1. Synthesis of diamine with naphthyl pendent group.

Scheme 2. Reaction scheme for preparing PI/ZnO hybrid thin films.

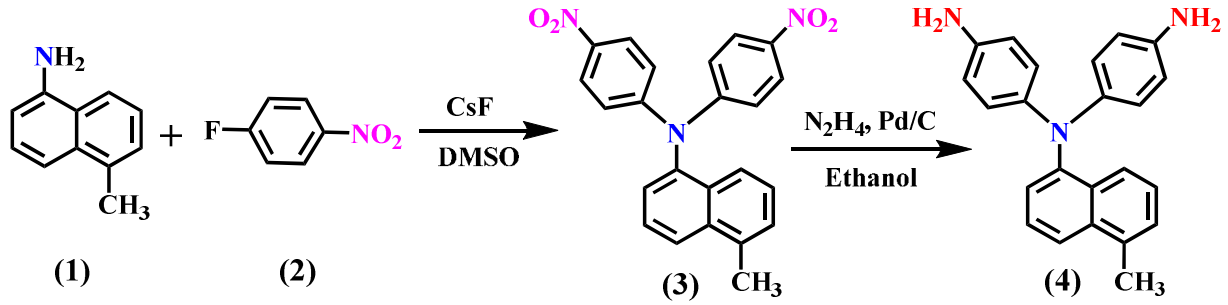

Scheme 1

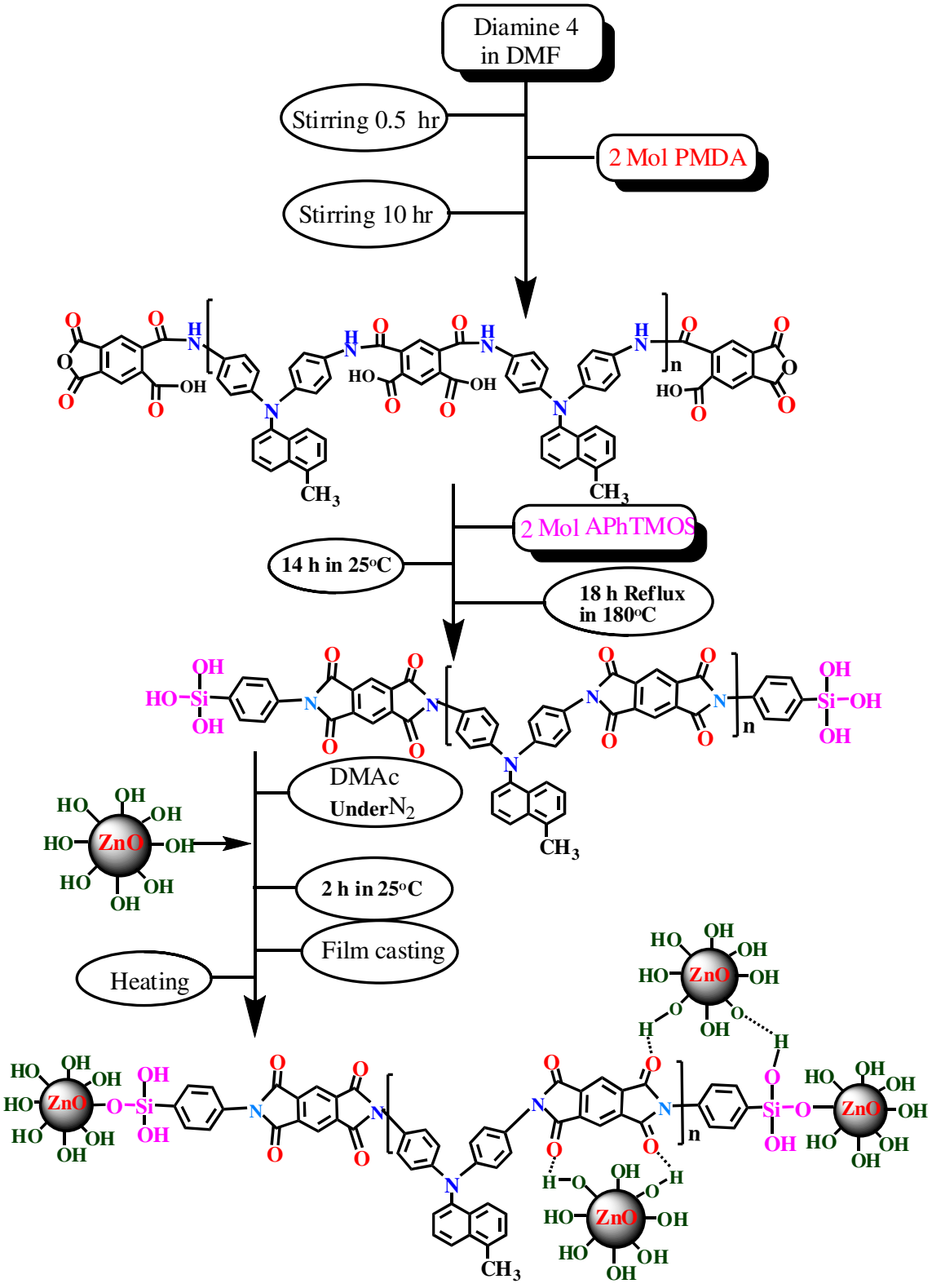

Scheme 2

Table 1 Thermal characterization of PI/ZnO NC films

Entry	Material	T_{10}[a] (ºC)	Char yield (%)[b]	T_g[c](°C)
1	Pure PI	416	67	142.7
2	PI/ZnO(5%)	448	74	147.2
3	PI/ZnO(10%)	496	77	154.3
4	PI/ZnO(15%)	532	81	161.5

[a]Temperature at which 5 and 10% weight loss was recorded by TGA at a heating rate of 20ºC/min in a nitrogen atmosphere.
[b] Percentage weight of material left undecomposed after TGA analysis at maximum temperature 800ºC in a nitrogen atmosphere
[c] Measured at a heating rate of 20 °C min^{-1} under N_2 atmosphere

Table 2 Mechanical properties for PI with various ZnO compositions

Entry	Material	modulus[a] (Mpa)	ultimate strength[b] (MPa)	ultimate elongation[c] (%)
1	Pure PI	3210.1	110.14	13.88
2	PI/ZnO (5%)	3535.6	118.22	10.97
3	PI/ZnO (10%)	3765.5	120.12	9.78
4	PI/ZnO (15%)	3899.3	123.20	9.11

[a] Initial slope of the stress strain curve. [b] Stress at break. [c] Elongation at break.

Table 3 Gas transport characteristics of PI and NC membranes

Sample	$P(O_2)$	$P(N_2)$	$P(CO_2)$	$P(CH_4)$	Ref
PI	3.97	1.81	19.81	3.76	
PI-ZnO(5%)	4.99	2.34	24.99	5.03	
PI–ZnO(10%)	5.62	2.59	29.02	5.98	
PI–ZnO(15%)	6.68	2.91	34.22	6.91	
Matrimid	1.90	0.27	8.70	0.24	43

Permeability coefficient (P) in barrer (1 barrer) 1 cm^3 (STP) cm cm^{-2} s^{-1} $cmHg^{-1}$ $\times 10^{-10}$), measured at 25 [o]C under an upstream pressure of 4 bar.

Table 4 Gas selectivity coefficients of PI with various ZnO compositions

Sample	Selectivity								
	O_2/N_2			CO_2/N_2			CO_2/CH_4		
	4bar	8bar	12bar	4bar	8bar	12bar	4bar	8bar	12bar
PI	2.19	2.20	2.22	10.80	11.67	12.03	5.29	5.67	5.78
PI–ZnO(5%)	2.13	2.15	2.17	10.55	11.41	12.14	5.22	5.41	5.59
PI–ZnO(10%)	2.17	2.25	2.30	10.64	12.30	12.75	4.85	5.39	5.48
PI–ZnO(15%)	2.30	2.20	2.29	11.77	12.03	9.25	4.95	5.10	5.39

Legends for Figures

Fig. 1. ^{1}H-NMR (500 MHz) spectrum of diamine 4 in DMSO-d_6 at R.T.

Fig. 2. ^{13}C-NMR (125 MHz) spectrum of diamine 4 in DMSO-d_6 at R.T.

Fig. 3. FT-IR spectra of the (a) PI/ZnO NC5%, (b) PI/ZnO NC10%, (c) PI/ZnO NC15%, (d) pure PI and (e) PAA.

Fig. 4. XRD patterns of pure PI and NC hybrid films with different amount of ZnO nanoparticles.

Fig. 5. FE-SEM micrographs of (a, b) PI/ZnO NC5% and (c, d) PI/ZnO NC15%.

Fig. 6. TEM micrographs of (a) PI/ZnO NC5% and (b) PI/ZnO NC10%.

Fig. 7. TGA thermograms of pure PI and hybrid films with different amount of ZnO nanoparticles.

Fig. 8. Tensile stress-strain curves of the pure PI and NC hybrid films with different amount of ZnO nanoparticles**.**

Fig. 9. Permeability of CO_2 in PI and PI/ZnO hybrid membranes.

Fig. 10. Permeability of CH_4 in PI and PI/ZnO hybrid membranes.

Fig. 11. Permeability of N_2 in PI and PI/ZnO hybrid membranes.

Fig. 12. Permeability of O_2 in PI and PI/ZnO hybrid membranes.

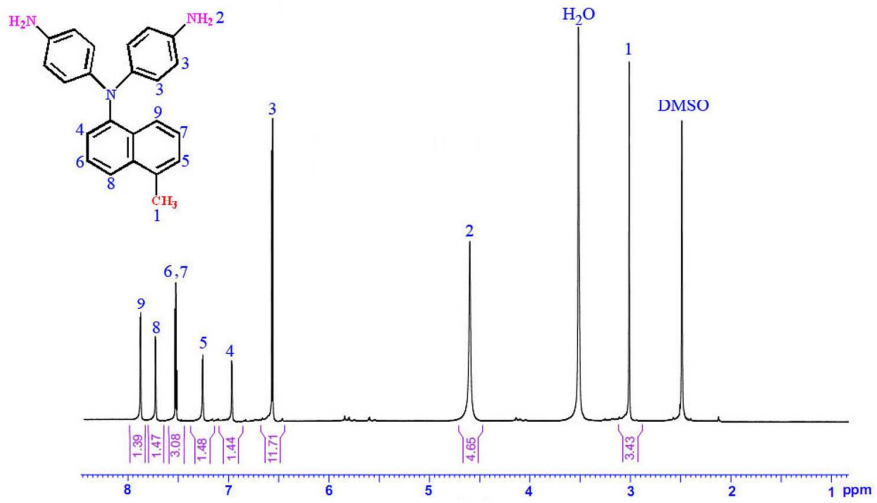

Fig. 1

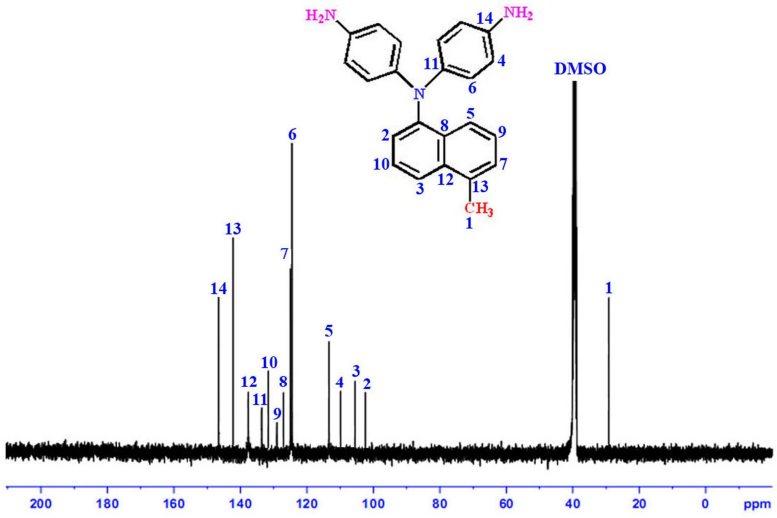

Fig. 2

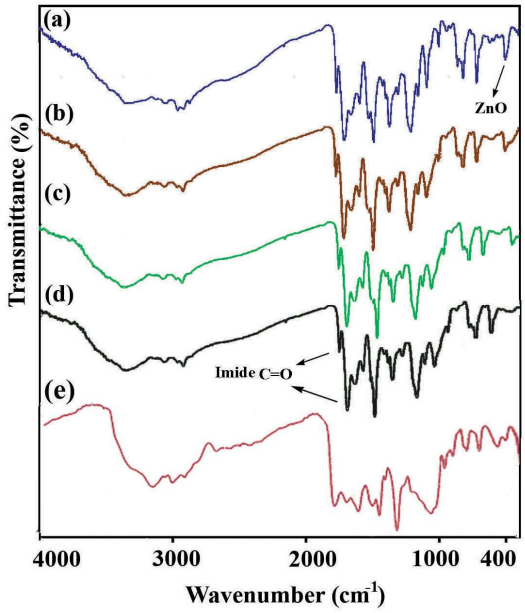

Fig. 3

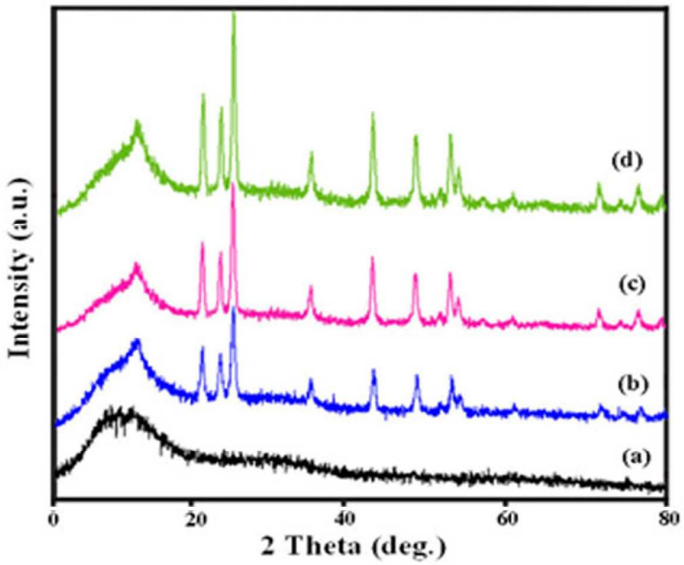

Fig. 4

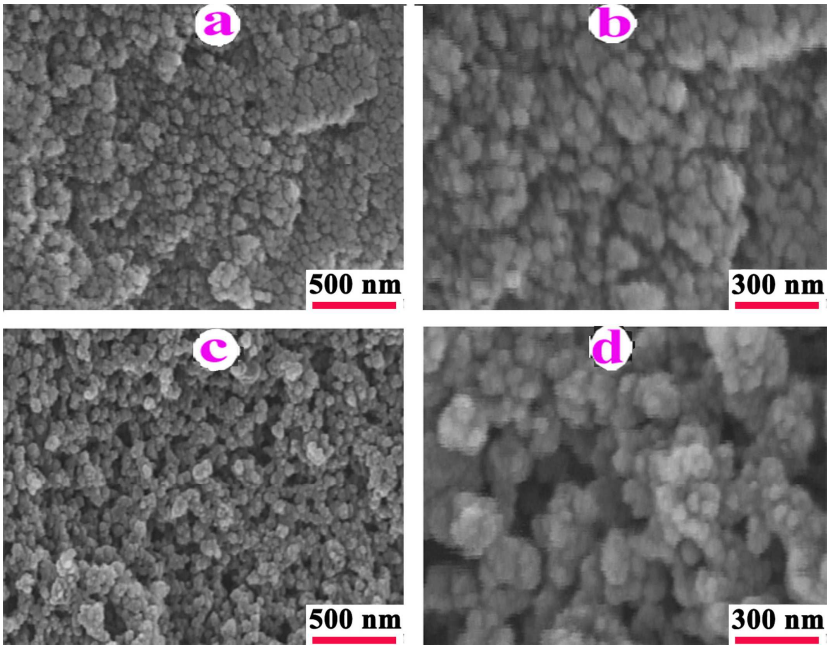

Fig. 5

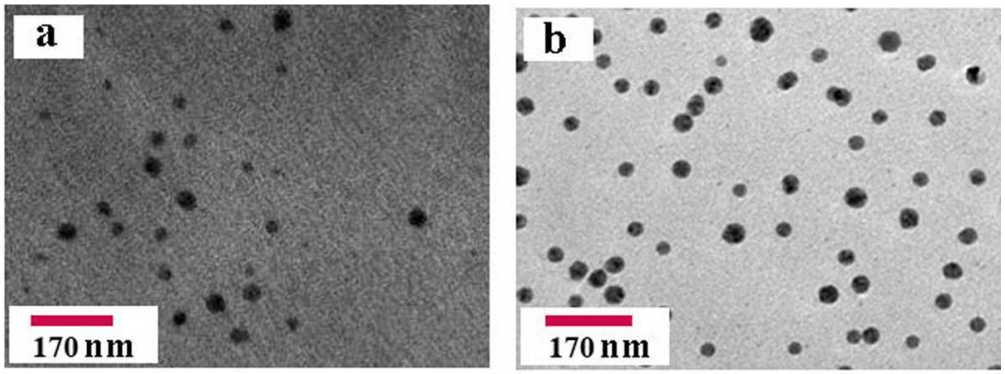

Fig. 6

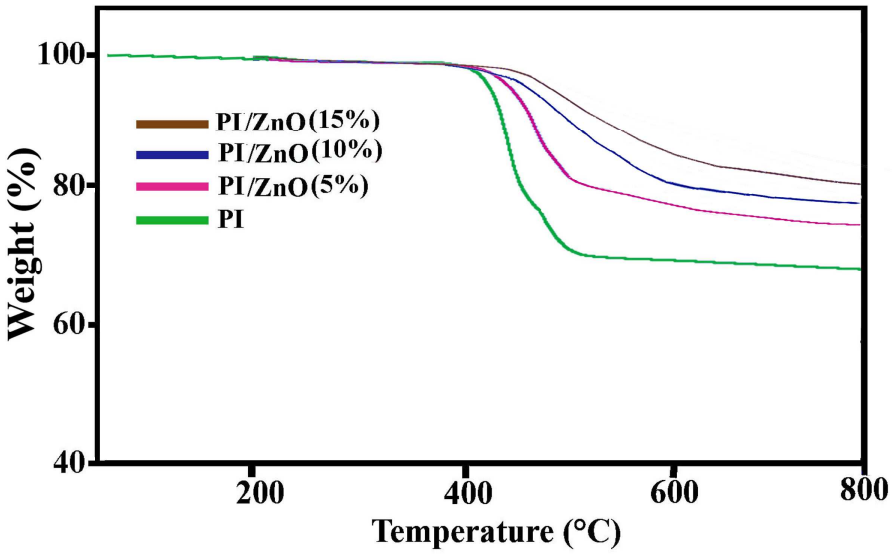

Fig. 7

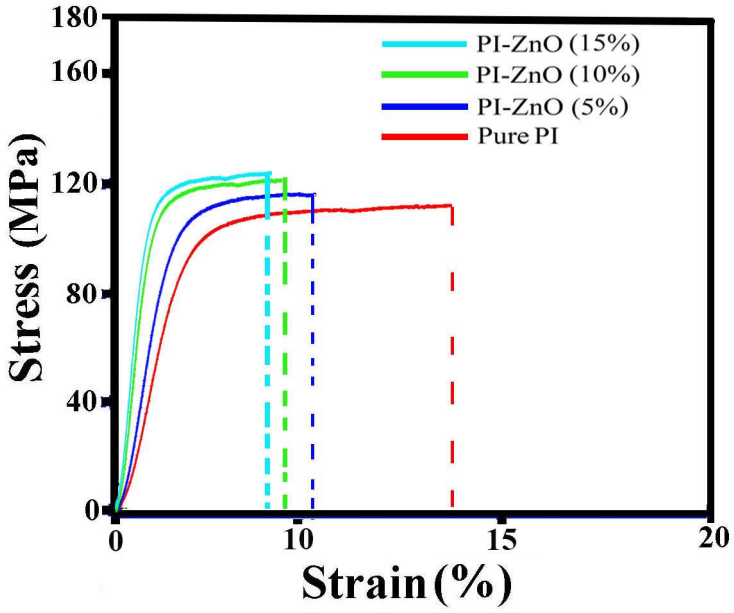

Fig. 8

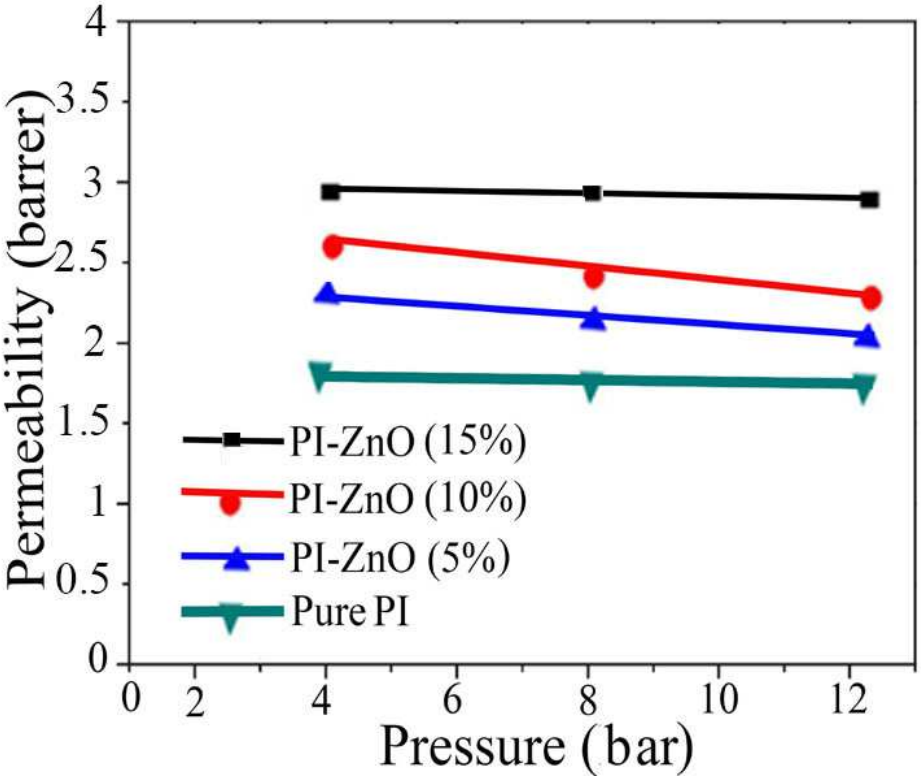

Fig. 9

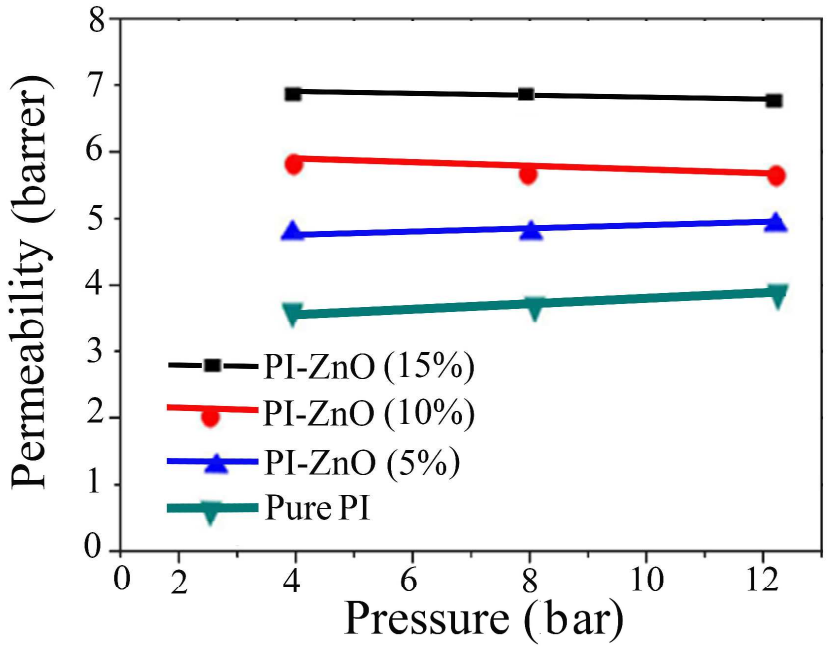

Fig. 10

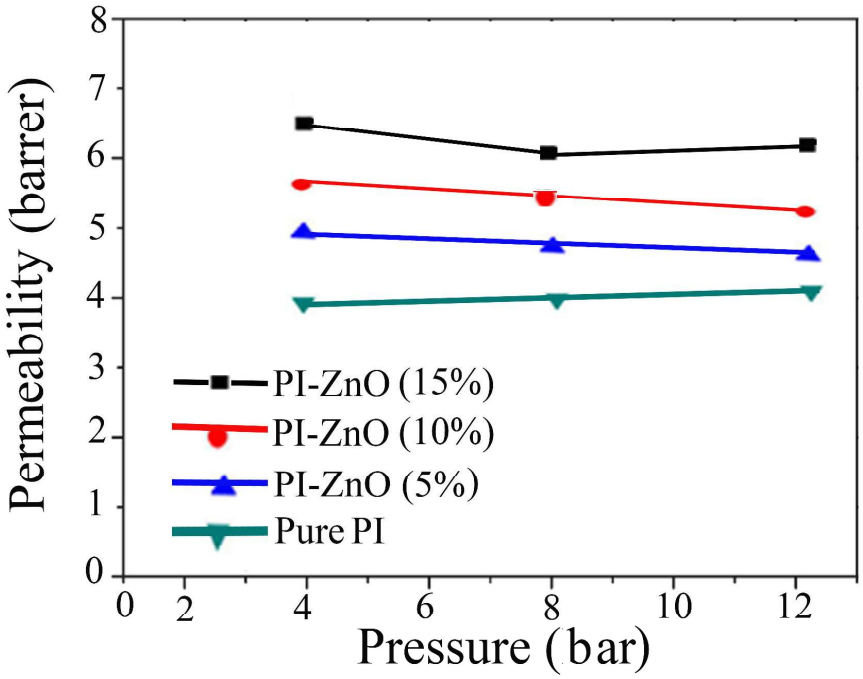

Fig. 11

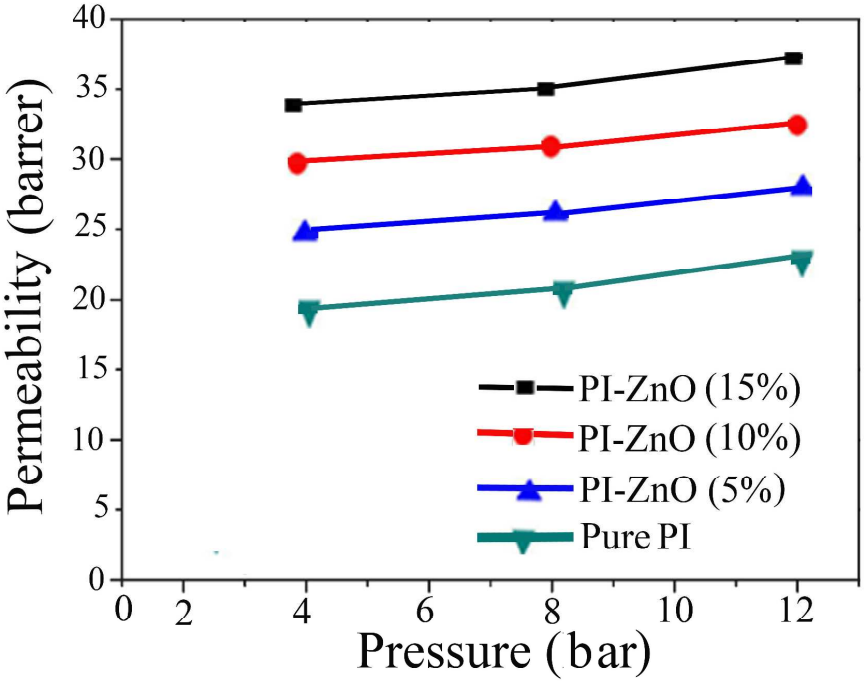

Fig. 12